Available online at www.sciencedirect.com

ScienceDirect

Procedia Manufacturing 41 (2019) 460–467

Procedia MANUFACTURING

www.elsevier.com/locate/procedia

8th Manufacturing Engineering Society International Conference

Experimental study of the compression behavior of mask image projection based on stereolithography manufactured parts

M. Casafont[a]*, J.M. Pons [a], J. Bonada [a], M.M. Pastor [a], F.Marimon [a], F. Roure [a]

[a]*DRMEE-ETSEIB Universitat Politècnica de Catalunya, Av. Diagonal 647, Barcelona, 08028, Spain*

Abstracts

The article presents the results of a series of compression tests on samples manufactured by means of the mask image projection based on stereolithography additive manufacturing technique (MIP-SL). Recent studies demonstrate the orthotropic nature of the MIP-SL materials. A research is initiated by the authors to attempt to predict the degree of anisotropy from the manufacturing parameters of the MIP-SL parts. The article focuses mainly on the development of the experimental compression tests of the first stage of the research. Special attention is paid to the four methods used to obtain the stress-strain curve of the material: strain gages, 2D Digital Image Correlation, extensometer measurements and crosshead displacement measurements. The article shows the advantages and limitations of each method. Finally, the anisotropic behaviour is verified and a testing procedure is set to obtain the constitutive parameters of the MIP-SL tested materials.

Keywords: Mask image projection stereolithography; Direct light processing (DLP); Digital image correlation (DIC)

1. Introduction

The research presented is focused on the study of the mechanical properties of parts produced by means of mask image projection based on stereolithography (MIP-SL). MIP-SL is an additive manufacturing technique where 3D objects are produced from photopolymer resins using a Direct Light Processing device (DLP). In this manufacturing process, the CAD model of the object is converted into a series of cross-sectional slices that, afterwards, are sequentially

* Corresponding author. Tel.: +34-93-4016589.
E-mail address: miquel.casafont@upc.edu

© 2019 The Authors. Published by Elsevier B.V.
This is an open access article under the CC BY-NC-ND license (http://creativecommons.org/licenses/by-nc-nd/4.0/)
Peer-review under responsibility of the scientific committee of the 8th Manufacturing Engineering Society International Conference.

projected onto the resin. The object is generated layer by layer in a printer like the one shown in Fig. 1. It can be observed that light is first projected on a Digital Micromirror Device (DMD), and then reflected in a container where the resin is located. The DMD consists of a series of micromirrors whose orientation may change. Depending on the orientation, the light is reflected into or out of the resin. Those mirrors that focus the light on the resin will create the shape of each layer after sufficient exposure time.

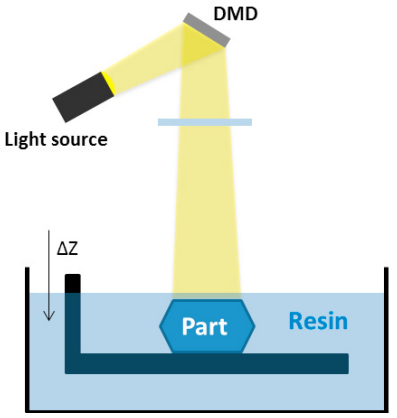

Fig. 1. Configuration of a top-down DLP printer.

Recent investigations demonstrate the anisotropic nature of the MIP-SL materials [1], which has been measured in parts subjected to tension [2-4] and bending [5,6]. The anisotropic behavior is caused by i) the pixels of the DLP device, that set a pattern of non-uniform photo-polymerized rectangles on the manufacturing plane of the part; ii) the interface between layers; and iii) the non-uniform polymerization through the layer thickness.

The next step in the research of DLP materials may be to attempt to predict the degree of anisotropy from manufacturing parameters. This is the main focus of the study recently initiated by the authors. A model capable of predicting the light energy dose that each part of the resin will receive during manufacturing is being developed. The first results can be found in [7,8]. From the output of this model, it is expected that it will possible to predict the degree of resin conversion and, consequently, the corresponding material properties at the different points of the object. Finally, the idea is that the anisotropic constants of the material will be estimated by means of a representative element volume (REV), whose material properties will be defined according to the light energy dose of each point.

The present article shows the first steps of the investigation, in which a set of samples have been manufactured using an energy dose according to the model developed. The main focus herein is the experimental tests carried out to assess the anisotropy of the resulting material. On the one hand, the experimental behavior of the material subjected to compression in different directions is studied. On the other hand, it has been considered interesting to include a short study of four different methods used to measure the stress-strain curve of the compressed specimens: strain gages, Digital Image Correlation (DIC), extensometer measurements and machine crosshead displacement measurements.

2. Materials and methodology

2.1. Test specimens

The test specimens were made from an acrylate photoactive resin (Spot HT from Spot-A Materials [9]). The shape and dimensions of the sample were set according to ASTM D 695-15 [10] (See Fig. 2a).

The specimens were manufactured in a top-down printer (Fig. 1), using a visible light source with a pixel resolution of 62.5 μm. All samples were printed with the same settings: a layer thickness of 75 μm and a controlled temperature of 23 ºC (see [7] for further details on the manufacturing process). More than one specimen was produced simultaneously. As a consequence, they were printed in different locations of the manufacturing platform. The print parameters were chosen so that all points of the sample could achieve full conversion according to the model presented

in [7]. Post-curing was not applied to the samples because it can cause changes in the resulting pattern of pixels and layers, which is actually what the authors want to study.

Since one of the objectives of the research is to assess the anisotropy of the material, samples were manufactured in different directions. In fact, it is assumed that the behavior of the material will be orthotropic. Consequently, the number of directions to be tested is six (X, Y, Z, XY, XZ and YZ in Fig. 2b), which provides sufficient data to calculate the 9 material constants of the corresponding constitutive law [11,12]. It is noted, however, that the full set of orthotropic constants is not determined in the present article. This will be done in the near future once the transverse strains are analyzed. The elastic moduli are only studied herein, which have been directly determined from the normal stress to longitudinal strain ratio measured for the X, Y, Z directions. Minimum 5 specimens of each manufacturing direction were tested, following ASTM standard [10].

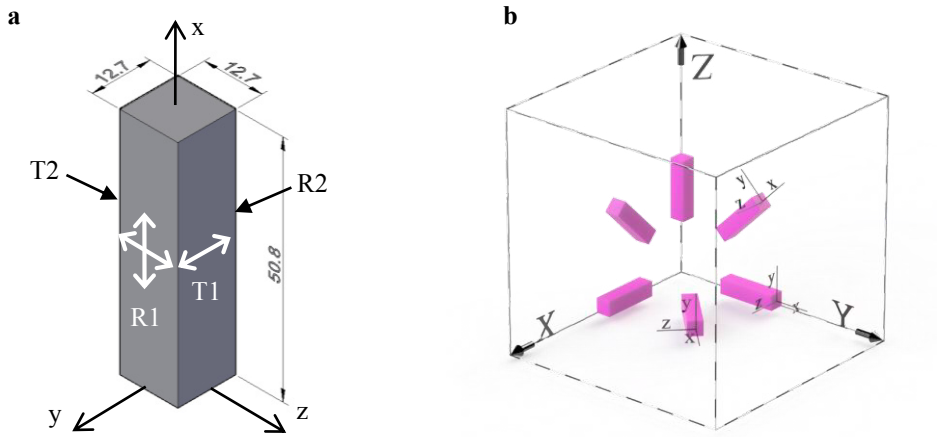

Fig. 2. (a) specimen (dimensions in mm.); (b) manufacturing directions XYZ and local coordinate systems xyz.

2.2. Experimental tests

Compression tests are performed in an Instron 3366 universal testing machine with a load capacity of ±10 kN. The loading rate is 2.6 mm/min. The test setup can be observed in Fig. 3a. As mentioned above, four different methods are applied to measure the strains that are used to plot the stress-strain curves. These methods are subsequently presented:

- General purpose strain gages. Each side of the specimen is equipped with strain gages. There are two sides, R1 and R2 in Fig. 2a, where two strain gage rosettes (TML FCA-2-11) are glued; and two other opposite sides, T1 and T2, with simple strain gages (TML FLA-2-11). The strain values are obtained by averaging the measurements corresponding to two opposite gages. This gage system provides the strains in one longitudinal (x) and two transverse directions (y and z).
- 2D-DIC. The strain field is measured in one of the sides of the specimen by means of a 2D Digital Image Correlation system. A 12 megapixel camera is used (4104x3006 pixel), that is located at 140 mm from the tested specimen. The strains are measured in a central portion of the specimen, far from the end sections and the strain gages, as can be seen in Fig. 3b. The measuring area is approximately equal to 12x12 mm (the width of the specimen is 12.7 mm). The number of pixels used in this area is about 1600x1130. The system provides one longitudinal strain (x) and one transverse strain (y).
- Extensometer. Strains are also determined from an extensometer that measures the shortening of the central part of the specimen (Fig. 3b). The extensometer measurement allowed the authors to calculate one longitudinal strain (x). It should be noted that only specimens Z, YZ and XZ were tested with extensometer.
- Crosshead displacement. Finally, the strains are also determined from the shortening of the specimen measured by the crosshead vertical displacement of the testing machine, which was recorded during the test. Only an estimation of the longitudinal strain (x) can be obtained with the crosshead.

The experimental stresses were calculated from the compression force measured by means of a load cell, and the experimental cross-section area of the specimens.

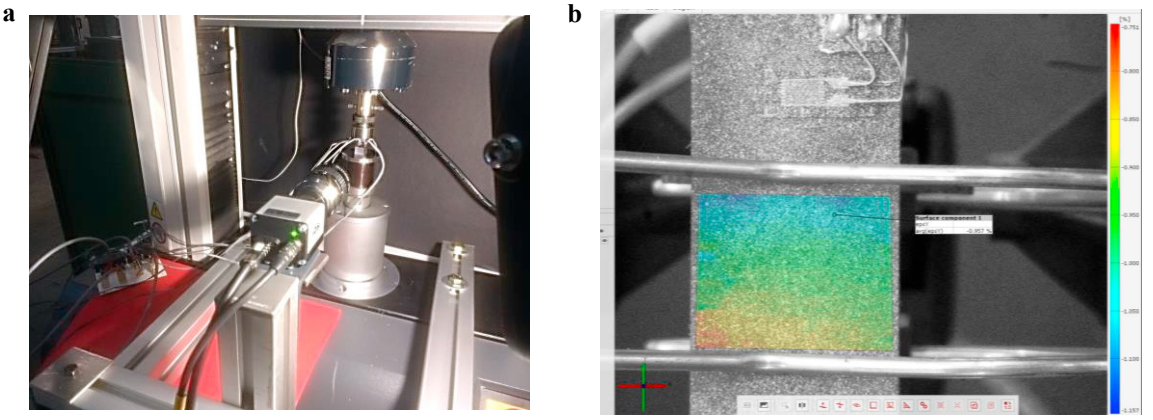

Fig. 3. (a) test setup; (b) 2D-DIC zone of measurement.

3. Results and discussion

3.1. General behavior

Firstly, the results of the tests on Z samples (manufactured on the Z direction, Fig. 2b) will be shown and discussed. Nine Z specimens have been tested using the four strain measuring methods presented in the previous section.

The graph of Fig. 4a shows the four different stress-strain curves obtained for specimen Z9. It can be observed that the strain gages are only able to provide data for the initial part of the curve. The strain gages are saturated or de-bonded just after reaching the yield stress, where the curve starts flattening. On the other hand, it should be pointed out that the extensometer was removed from the specimen at a low load level to avoid any damage in case of sudden and violent fracture. This is the reason why the corresponding curve is also truncated well before the end of the test. The 2D-DIC and the crosshead curve were able to follow the test until the end. The test stopped when the maximum load capacity of the machine was achieved.

Most of the samples did not show failure (shattering failure). For this reason, the compressive stress in Fig. 4a rises steadily, without any well-defined fracture occurring. This is in accordance with what it is expected in [10].

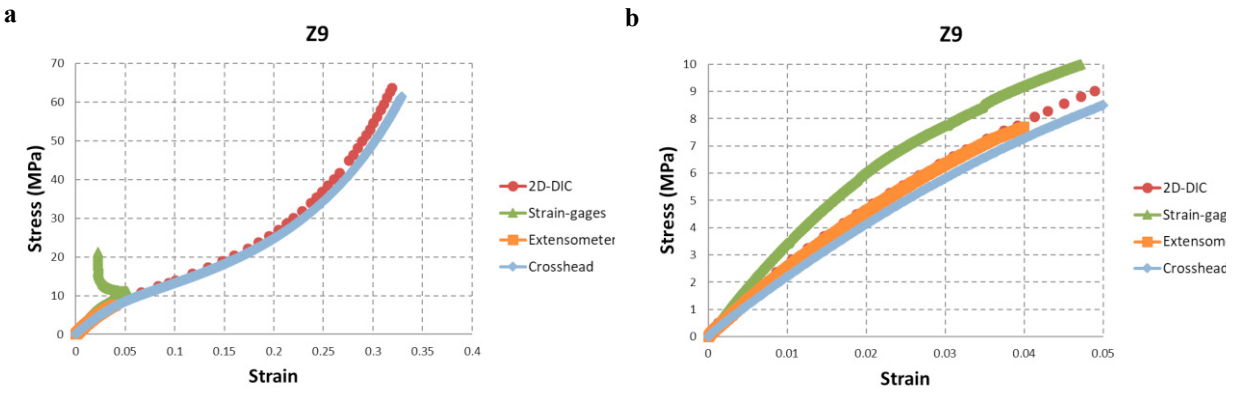

Fig. 4. (a) Stress-strain curves of Z9 specimen; (b) initial portion of the Z9 stress-strain curves.

A first remark on the accuracy of the four stress-strain curves can already be done from Figs. 4a and 4b. It seems that the 2D-DIC, the extensometer and the crosshead produces rather similar curves for the specimens Z9, especially at the beginning of the tests. 2D-DIC and crosshead measurements diverge a little bit at the end. This is reasonable because the specimens usually showed bending at advanced stages of the loading process, which cannot be captured by means of the crosshead measurements. On the other hand, it can also be observed that the strain gage curve goes slightly above the other curves.

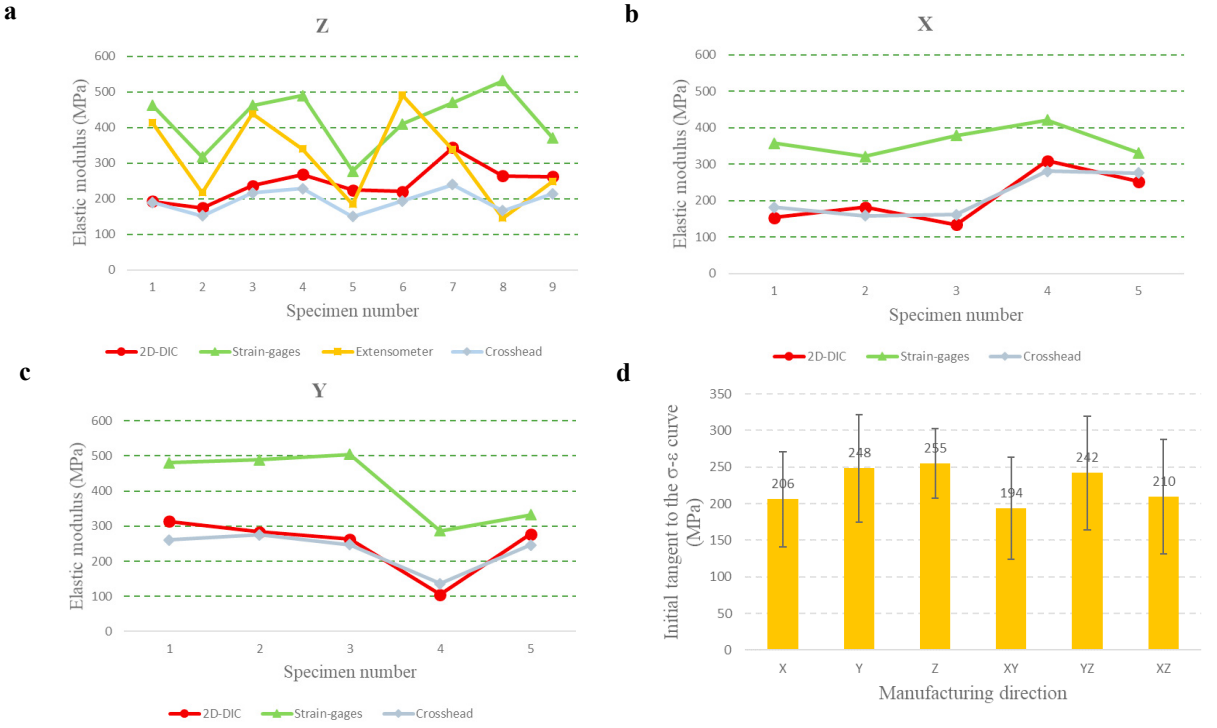

Fig. 5. Elastic moduli: (a) Z samples; (b) X samples; (c) Y samples; (d) Mean values of the initial tangent to the stress-strain curve (the first three columns correspond to the X, Y and Z elastic moduli).

3.2. Calculation of the elastic modulus

The elastic moduli were determined by calculating the tangent to the initial part of the stress-strain curves (Fig. 4b), following the recommendations of [10]. The elastic modulus of each specimen is the average of the tangents obtained on point-by-point increasing ranges of curve values. The starting point considered was a strain value of 0.001, and the ending point the one at which the new tangent differed by more than 5% from the averaged one (see [13]). If the number of averaged tangents was lower than 10, the starting point increased to a new value (maximum starting point was 0.01).

Fig. 5a shows the values corresponding to the nine Z specimens, which have been calculated considering the four different experimental stress-strain curves. It can be observed that the dispersion is rather high (see also PD and CV in Table 1), mainly when the modulus of elasticity is determined from extensometer data (PD = 32 % and CV=39 %). Dispersion is lower when the calculation is carried out from 2D-DIC and crosshead measurements (PD and CV around 15 % and 19 %, respectively). These two techniques produce higher dispersion when the X and Y elastic moduli are determined, see Table 1 (PD and CV in the range of 20 % to 30 %). However, since both methods result in very similar elastic moduli, see Fig. 5b, Fig. 5c and first specimens in Fig. 5a, it might be concluded that the dispersion is due to the nature of the specimens, and not to the measuring system. On the other hand, the dispersion of the elastic moduli obtained from the strain gage measurements is slightly lower to that resulting 2D-DIC and crosshead (see also Table 1). It seems a more robust measuring method. The problem with the strain gage measurements is that they produce

higher elastic moduli than those obtained by the other techniques for all X Y and Z samples. This is in line with the specialized literature [14], that shows that strain gages may stiffen the material when its elastic modulus is below 1000 MPa, as in the present study.

The 2D-DIC values are considered to assess the anisotropic nature of the material. The averaged values (and dispersion) of the tangent to the initial part of the stress-strain curves of the six manufacturing directions tested are shown in Fig. 5d. If one focus on the values corresponding to the X, Y and Z directions, which are the three elastic moduli, it can be concluded that the material can be considered anisotropic. The elastic modulus ratios (E_i/E_j) range from 0.81 to 0.97.

Finally, it should be pointed out that the resulting elastic moduli are lower than expected according to previous tests on post-cured samples [15], and other data from existing literature [2-6]. This can be attributed to the fact that in the present research the manufacturing procedure is different (for instance, no post-curing is applied), and the loading conditions are not the same in the previous studies. The authors also believe that the model used to set the energy dose, that is considering a uniform energy distribution in the projected DMD pixels (see [7]), has an influence. In reality, the energy dose is non-uniform [16], which causes non-uniform material properties within the pixel. Some parts of the pixels have lower properties than the predicted values, resulting in a lower overall performance of the material.

Table 1. Mean values of measured elastic moduli (E) and calculated statistical parameters.

Manufacturing direction	Measuring technique	Mean of E (MPa)	Average deviation (MPa)	PD: Percent deviation (%)	Standard deviation (MPa)	CV: Coefficient of variance (%)
Z	2D-DIC	255	38	15	50	20
	Strain gages	421	69	16	84	20
	Extensometer	313	101	32	121	39
	Crosshead	194	27	14	33	17
X	2D-DIC	206	60	29	65	27
	Strain gages	362	31	8	36	10
	Crosshead	211	53	25	55	26
Y	2D-DIC	248	57	23	74	33
	Strain gages	419	87	21	91	12
	Crosshead	233	39	17	49	21

3.3. Additional information from 2D-DIC measurements

To close this Section, it is believed worth to discuss three pictures obtained by means of the 2D-DIC technique that support some of the decisions taken above:

- Fig. 6a shows the longitudinal strains (x) measured in specimen YZ3. The strain measurements include the portion where the strain-gage is located. It can be observed that the strain gage is a singularity that stiffens. The strains in the gage are lower than in other parts of the central zone of the sample.
- In Fig. 7, the stress-strain curve resulting from a 2D-DIC measurement onto the strain gage is compared with the strains measured by the strain gage, and the 2D-DIC measurement in the central portion of the sample. The two first curves are similar, and higher than the last one, which supports the remark of the previous point. It should be noted that such agreement between DIC in R1 and strain gage values could not be obtained for all samples.
- It is interesting to see in Fig. 6b how a cracked sample behaves. To detect cracked samples using DIC was useful in the study. It allowed the authors to know why certain measured elastic moduli were excessively low.

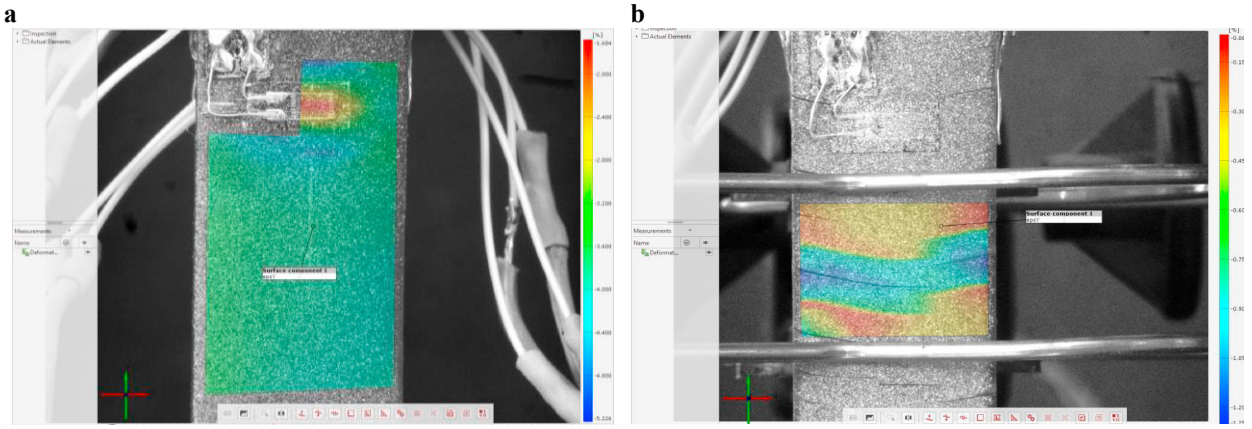

Fig. 6. 2D-DIC strain field in: (a) a strain gage; (b) a cracked specimen.

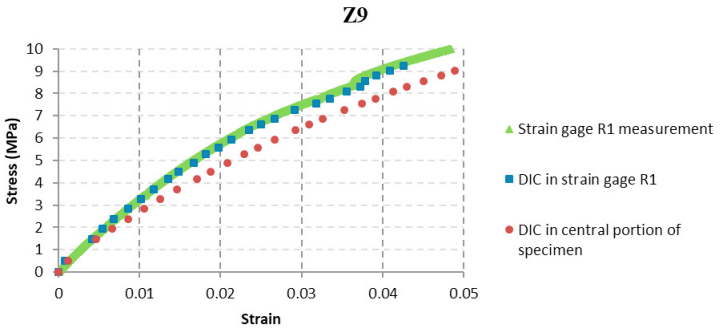

Fig. 7. Initial stress-strain curve of the Z9 specimen.

4. Conclusions

The article has presented an experimental study of the compression behavior of MIP-SL materials. The values of elastic modulus measured showed high dispersion, but the trend observed in Fig. 5d seems to confirm the anisotropic nature of the specimens. It is interesting to highlight that anisotropy is more significant in the XY manufacturing plan than in the Z manufacturing direction (see also [5]). This means that the layer effect, connection effect between manufacturing layers, is less important than the pixilation effect, i.e. the effect of the non-uniform photo-conversion distribution of the material within projected DMD pixels. It is also worth to note that the elastic moduli finally obtained are lower than expected. This is also attributed to the pixilation effect, which had not been taken into account in the model developed to set the energy dose during manufacturing [7]; and to the fact that no post-curing was applied to the samples.

In the near future, research will focus on improving the energy model so that pixilation is included and better predictions of the mechanical properties are obtained. So far, the model developed under the assumption of uniform energy of the pixel has been good enough to produce parts with geometric accuracy [7]; but it seems that a more sophisticated approach for the pixel energy distribution needs to be considered to produce parts with the desired mechanical behavior. On the other hand, the effect of post-curing will also be studied. However, it is expected that it will be difficult to remove the pattern of pixels by means of post-curing due to the large thickness of the samples.

The article also included a comparative study of different experimental techniques to measure the stress-strain curves of the material. The performance of the 2D-DIC, strain gage and crosshead measuring methods is similar. The 2D-DIC results were finally chosen to assess the degree of anisotropy of the material, because i) it is a non-contact technique (no stiffening effect occurs), and ii) it provides the full 2D strain field, that will be used in the future to

derive Poisson ratio values. The main disadvantage of the DIC process is that it is a bit demanding in post-processing. Efficient DIC software is needed, which may be an issue when 3D-DIC analyses are to be performed. For 2D-DIC analysis there a number of free programs that can easily be applied (in the present study the GOM correlate free 2D-DIC software was used [17]). Concerning the other measuring techniques, it can be concluded that: i) the strains derived from the crosshead displacements are similar to the 2D-DIC strains. The main limitation of this measurement procedure is that it only allows deriving the axial strain of the sample. Another limitation, which was not relevant in the present study, is that no direct measurement on the material is carried out and, consequently, the real behavior of the sample may not be captured; ii) the dispersion of the elastic moduli obtained from the extensometer measurements is higher. Nevertheless, it should be highlighted that this measurement technique resulted very practical because it needs neither preparation of the sample nor a costly post-processing of the experimental data; iii) the strain gage elastic modulus dispersion is slightly lower to the DIC and extensometer dispersions. The main disadvantages of the strain gage system are the sample preparation cost, and the limited measuring range due to saturation and de-bonding. Another problem that may be encountered when working with flexible materials is the stiffening effect of the strain gage. This can be solved by using a correction factor, as discussed in [14]. In the present study, the strain gages were the only system that allowed direct measurement of the strains in the three orthogonal directions of the sample.

Acknowledgements

Authors would like to thank the Spanish Ministry of Economy and Competitiveness for the financial support to the research project “Nuevas tecnologias para la impresion 3D de materiales avanzados” (DPI2016-80119-C3-2-R). The author J.Bonada is a Serra Húnter Fellow.

References

[1] J.R.C. Dizon, T. A.H. Espera Jr., Q. Chen, R.C. Advincula, Mechanical characterization of 3D-polymers, Additive Manufacturing, 20 (2018) 44-67.
[2] E. Aznarte, C. Ayranci, A.J. Qureshi, Digital light processing (DLP): anisotropic tensile considerations, Solid Freeform Fabrication 2017: Proceedings of the 28th Annual Freeform Fabrication Symposium – An Additive Manufacturing Conference, (2017) 413-425.
[3] E. Aznarte, A.J. Qureshi, A study on material-process interaction and optimization for VAT-photopolymerization processes, Rapid Prototyping Journal, 24/9 (2018) 1479-1485.
[4] N.H. Chang, S.E. Song, K. Park, Investigation on anisotropy according to printing conditions for projection type photo-polymerization 3D printing, Polymer (Korea), Vol. 42, No. 6 (2018) 1040-1045.
[5] M. Monzón, Z. Ortega, A. Hernández, R. Paz, F. Ortega, Anisotropy of photopolymer parts made by digital light processing, Materials, 10, 64 (2017).
[6] M. Hatzenbichler, M. Geppert, R. Seemann, J. Stampfl, Additive manufacturing of photopolymers using the Texas Instruments DLP Lightcrafter, Proceedings of the SPIE-The International Society for Optical Engineering (2013).
[7] J. Bonada, A. Muguruza, X. Fernández-Francos, X. Ramis, Optimisation procedure for additive manufacturing processes based on mask image projection to improve Z accuracy and resolution, Journal of manufacturing processes, 31 (2018) 689-702.
[8] J. Bonada, E. Xuriguera, A. Muguruza, J. Gonçalves, P. Barcelona, J.M. Pons, J. Minguella, R. Uceda, Reinforced photocurable materials for additive manufacturing process based on mask image projection, Submitted to Procedia Manufacturing (Mesic 2019).
[9] Spot-A materials: https://spotamaterials.com/ (Last accessed on 26 February 2019).
[10] ASTM D695-15, Standard test method for compressive properties of rigid plastics, ASTM International (2015).
[11] R. Zou, Y. Xia, S. Liu, P. Hu, W. Hou, Q. Hu, C. Shan, Isotropic and anisotropic elasticity and yielding of 3D printed material, Composites Part B, 99 (2016) 506-513.
[12] S.G. Lekhnitskii, Theory of elasticity of an anisotropic body, Mir Publishers, Moscow (1981).
[13] S. Brischetto, C.G. Ferro, P. Maggiore, R. Torre, Compression tests of ABS specimens for UAV components produced via the FDM technique, Technologies, 5, 20 (2017).
[14] A. Ajovalasit, L. D’Acquisto, S. Fragapane, B. Zuccarello, Stiffness and reinforcement effect of electrical resistance strain gauges, Strain, 43 (2003), 299-305.
[15] J. Bonada, A. Muguruza, X. Fernández-Francos, X. Ramis, Influence of exposure time on mechanical properties and photocuring conversion ratios for photosensitive materials used in additive manufacturing, Procedia Manufacturing, 13 (2017) 762-769.
[16] C. Zhou, Y. Chen, R.A. Waltz, Optimized mask image projection for solid freeform fabrication, Journal of manufacturing science and engineering, 131(6) (2009).
[17] GOM Correlate. GOM—Precise Industrial 3D Metrology. Braunschweig, Germany. Available online: https://www.gom.com/index.html (accessed on 5 March 2019).